



Synthetic conditions and their doping effect on β -K₂Bi₈Se₁₃

Th. Kyratsi^{a,*}, I. Kika^a, E. Hatzikraniotis^b, K.M. Paraskevopoulos^b, K. Chrissafis^b, M.G. Kanatzidis^c

^a Department of Mechanical and Manufacturing Engineering, University of Cyprus, 1678 Nicosia, Cyprus

^b Physics Department, Aristotle University of Thessaloniki, 54124 Thessaloniki, Greece

^c Department of Chemistry, Northwestern University, Evanston, IL 60208, and Materials Science Division, Argonne National Laboratory, Argonne, IL 60439, United States

ARTICLE INFO

Article history:

Received 17 April 2008

Received in revised form 18 June 2008

Accepted 20 June 2008

Available online 28 August 2008

Keywords:

Thermoelectric materials

Chemical synthesis

ABSTRACT

In this work the synthetic conditions for K₂Bi₈Se₁₃ and their effect on its thermoelectric properties were investigated. K₂Bi₈Se₁₃ was prepared as a single phase using K₂Se and Bi₂Se₃ as starting materials in a furnace or via a reaction using direct flame, followed by remelting or annealing. Seebeck coefficient measurements showed that the doping level in the material is sensitive to the synthetic conditions. Higher synthesis temperatures as well as the flame reaction technique followed by annealing gave more homogeneous samples with higher Seebeck coefficient. IR optical spectroscopic measurements showed a wide range of doping level achieved among the different synthetic conditions. These findings suggest that synthetic conditions can act as a useful tool for the optimization of the thermoelectric properties of these materials.

© 2008 Elsevier B.V. All rights reserved.

1. Introduction

The thermoelectric figure-of-merit ZT of a material is given by

$$ZT = \frac{S^2 \sigma}{\kappa} T \quad (1)$$

where σ is the electrical conductivity, S is the Seebeck coefficient, κ is the thermal conductivity and T is the temperature. Candidate materials for thermoelectric applications should possess high electrical conductivity, high Seebeck coefficient and low thermal conductivity, so the thermoelectric figure-of-merit ZT can be maximized exceeding one.

Research on complex bismuth chalcogenide compounds has shown that β -K₂Bi₈Se₁₃ has many attractive features that make it promising for thermoelectric applications [1–3]. The structure of β -K₂Bi₈Se₁₃ [4] include two different interconnected types of Bi/Se blocks, K ions positionally and compositionally disordered with Bi or other K atoms, over the same crystallographic sites, and loosely bound K atoms in tunnels. Decrease of the lattice thermal conductivity can be accomplished based on the concept of “phonon glass electron crystal” (PGEC) [5] through “rattling” atoms in cages or tunnels of the structure, or by materials with complex compositions, large unit cells, low crystal symmetry and site occupancy disorder provided. β -K₂Bi₈Se₁₃ combines such fea-

tures that seem to be responsible for its low thermal conductivity (~ 1.3 W/m K) [4].

Attempts to improve the thermoelectric properties of β -K₂Bi₈Se₁₃ have been done based on solid solution formation as well as doping experiments. Solid solutions were prepared via substitution on the heavy metal sites (i.e., K₂Bi_{8-x}Sb_xSe₁₃) [6,7], on the alkali metal site (i.e., K_{2-x}Rb_xBi₈Se₁₃) [8] as well as on the chalcogenide sites (i.e., K₂Bi₈Se_{13-x}S_x) [9]. The series were studied in terms of crystallography, physical and thermoelectric properties. Doping studies were also carried out on selected members using varying amounts of excess Se, Pb and Sn [6]. The charge transport properties of the K₂Bi_{8-x}Sb_xSe₁₃ series (low Sb concentration) as well as doped materials displayed degenerate semiconductor behavior with very high free carrier concentration of $\sim 10^{20}$ cm⁻³.

According to band structure calculations [10] there are special sites in the crystal structure that are very important for the properties of this material. The calculations indicated that, depending on how the K and Bi atoms are arranged in the mixed occupancy lattice sites, an energy gap may or may not appear at the fermi level. Therefore, two extreme variants of the band structure exist: from a semimetal (band overlap) to semiconductor (band gap) based on the K/Bi arrangements. Detailed analysis [11] of the carrier concentration as well as of the Seebeck coefficient had shown that the properties of Bi-rich members of the K₂Bi_{8-x}Sb_xSe₁₃ series were well described with a finite-gap semiconductor model that contained a significant concentration of shallow donors. We believe that these shallow donors that likely originate from defects created by local disordering between K and M (Bi, Sb),

* Corresponding author. Tel.: +357 22892267.

E-mail address: kyratsi@ucy.ac.cy (Th. Kyratsi).

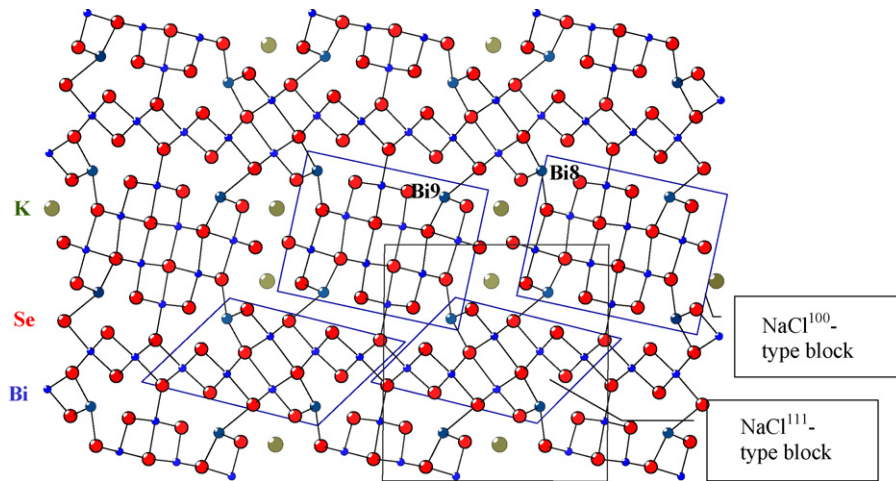


Fig. 1. Crystal structure of the β - $\text{K}_2\text{Bi}_8\text{Se}_{13}$ compound.

resulted in the difficulty to make materials with low carrier concentration.

In this work, we aimed to explore how the synthetic conditions affect the doping level of these materials in order to find a procedure that leads to promising and doping-sensitive materials. We studied the $\text{K}_2\text{Bi}_8\text{Se}_{13}$ compound with emphasis on modifying the free carrier concentration in order to find more efficient ways to control the doping level of the material through the synthesis procedure. We focused mainly on using K_2Se and Bi_2Se_3 as starting materials and treat them with different heating/cooling profiles. The products were studied with X-ray diffraction, thermal analysis and energy dispersive spectroscopy regarding their purity and elemental analysis while Seebeck coefficient and IR reflectivity measurements were performed in order to study their doping level and explore their properties.

2. Experimental

2.1. Reagents

Chemicals in this work were used as obtained: (i) bismuth metal, 99.999% purity, Alfa Aesar; (ii) Selenium metal, 99.999% purity, Alfa Aesar; (iii) potassium metal, rod, 99.5% purity, Aldrich Chemical Co.

2.2. Synthesis

$\text{K}_2\text{Bi}_8\text{Se}_{13}$ was synthesized using K_2Se and Bi_2Se_3 as starting materials and following different heating treatments as described below. All manipulations were carried out under nitrogen atmosphere. The reacting materials were sealed in silica tubes under vacuum (10^{-4} Torr). All products however are stable and can be handled and stored in air. K_2Se was prepared by stoichiometric combination of K and Se in liquid ammonia. Bi_2Se_3 was prepared by the stoichiometric combination of the elements at 900°C .

Table 1

Synthetic conditions for β - $\text{K}_2\text{Bi}_8\text{Se}_{13}$ and their minimum and maximum Seebeck coefficients

Sample	Synthetic condition	Temperature ($^\circ\text{C}$)/duration (h)	S_{max} ($\mu\text{V}/\text{K}$)	S_{min} ($\mu\text{V}/\text{K}$)
I-1	In furnace	760/0	-119.0	-57.8
I-2		760/3	-142.6	-95.6
I-3		780/0	-130.6	-89.5
I-4		820/0	-130.7	-116.9
I-5		820/1	-136.9	-115.9
I-6		850/1	-143.2	-127.7
II-1	Flame reaction + remelting	760/3	-131.9	-113.5
II-2		780/3	-162.5	-151.3
III-1	Flame reaction + annealing	500/48	-193.4	-184.0
III-2		500/60	-222.7	-204.9
III-3		500/76	-238.4	-223.2

2.3. Powder X-ray diffraction

The samples were examined by X-ray powder diffraction to assess phase purity. Powder patterns were obtained using a Rigaku Miniflex powder X-ray diffractometer with Ni-filtered $\text{Cu K}\alpha$ radiation operating at 30 kV and 15 mA. The data were collected at a rate of $0.5^\circ/\text{min}$. The purity of phases for the solid solutions was confirmed by comparison of X-ray powder diffraction pattern to the calculated one from single crystal data for β - $\text{K}_2\text{Bi}_8\text{Se}_{13}$ using Cerius² software [12]. The reported purity of phases is subjected to the detection limit of the experiment which is approximately 4%.

2.4. Thermal analysis

Differential scanning calorimetry (DSC) was performed with a computer-controlled SETARAM Setsys 16/18 TG-DTA as well as Linseis STA1600 thermal analyzer. The ground samples (~ 30 mg total mass) were placed in alumina crucibles and heated under argon flow to 730°C at $10^\circ\text{C}/\text{min}$.

2.5. Energy dispersive spectroscopy (EDS)

EDS was realized using a Jeol 840A scanning microscope with an energy dispersive spectrometer attached (Oxford, model ISIS 300). The beam spot was $1\ \mu\text{m}$, the accelerating voltage 20 kV, the beam current 0.4 nA, the working distance 20 mm and the counting time 60 s real time. The matrix correction protocol was ZAF correction.

2.6. Thermoelectric properties

Seebeck coefficient measurements were carried out at temperature range of 80–400 K with a programmable Seebeck controller SB100 from MMR Technologies, Inc., using constantan wire as reference. Heat gradient was applied along the needle direction (crystallographic b -axis).

2.7. Optical properties

Infrared spectra were recorded at nearly normal incidence in the 70 – $2000\ \text{cm}^{-1}$ spectral region, at room temperature, with a Bruker 113 V FT-IR spectrometer with a

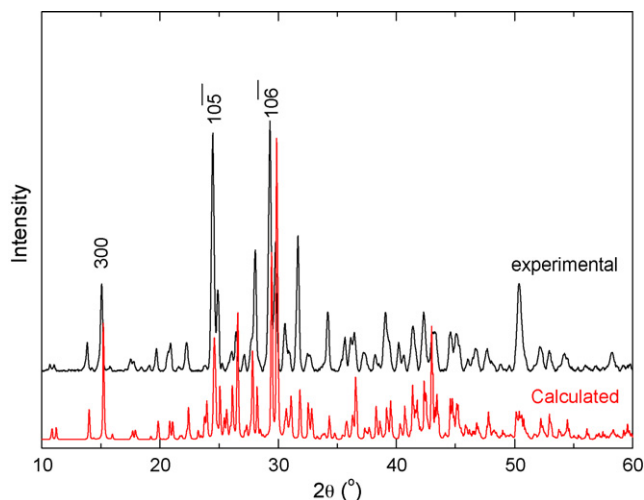


Fig. 2. Experimental XRD pattern of $K_2Bi_8Se_{13}$ compare to the calculated from Cerius software.

resolution of $\sim 2 \text{ cm}^{-1}$. The reflection coefficient was determined by typical sample-in-sample-out method with a gold mirror as the reference. Measurements were carried out on pressed pellets (crystals were first ground using mortar and pestle and then cold pressed).

3. Results and discussion

3.1. Structure of $K_2Bi_8Se_{13}$

The structure of $\beta\text{-}K_2Bi_8Se_{13}$ includes two different interconnected types of Bi/Se rod-shaped building blocks and K^+ atoms in tunnels [4], see Fig. 1. The so-called $NaCl^{(111)}$ -type Bi/Se building blocks are cuts representing Bi_2Te_3 -type structural fragments, interconnected to form a step-like structure along a -axis. $NaCl^{(111)}$ -type blocks are bridged, along c -axis, with the $NaCl^{(100)}$ -type Bi/Se building blocks that are separated by tunnels. The $NaCl^{(111)}$ -type and $NaCl^{(100)}$ -type blocks are connected on Bi(8) atom as well as at Bi(9) metal site with Bi–Se bonds. In this structure these connecting sites were found to be mixed occupied by K and Bi atoms and according to band structure calculations the electronic properties of the material are sensitive to the K/Bi atom distribution [10].

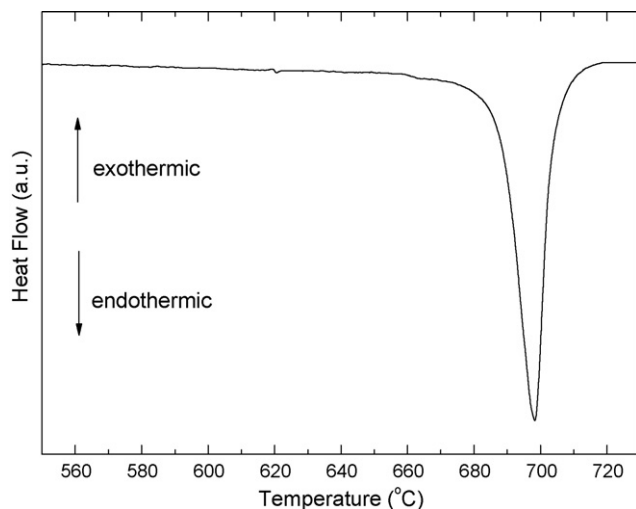


Fig. 3. DSC graph of $K_2Bi_8Se_{13}$ (sample from I-2).

3.2. Synthesis and characterization

Previously, $\beta\text{-}K_2Bi_8Se_{13}$ type materials were prepared by direct combination of the elements and were grown by Bridgman techniques [13]. The latter gives highly oriented large ingot samples. These samples show strong anisotropic properties and high free carrier concentration [6]. We have also reported solid solutions of $K_2Bi_8Se_{13}$ with Sb [6,11] and S [9,14] prepared by stoichiometric combination of the elements followed by Bridgman crystal growth. The Seebeck coefficient of the Bi-rich members of $K_2Bi_{8-x}Sb_xSe_{13}$ was below $-100 \mu\text{V/K}$ [6] and for $K_2Bi_8Se_{13-x}S_x$ it was $\sim -120 \mu\text{V/K}$ for $x=4$ [14]. Doping experiments were also carried out on $K_2Bi_{8-x}Sb_xSe_{13}$ with $x=1.6$ and the Seebeck coefficient was below $-90 \mu\text{V/K}$ using Pb and Sn as dopants. In general, all materials prepared by stoichiometric elemental combination followed by Bridgman crystal growth showed a relatively high doping state with carrier concentration [6] of the order of 10^{20} cm^{-3} . Those results suggest the $\beta\text{-}K_2Bi_8Se_{13}$ materials are not responsive to doping when they are prepared by Bridgman technique. Moreover, when $\beta\text{-}K_2Bi_8Se_{13}$ was prepared using K_2Se , Bi and Se metals as starting materials [4], lower carrier concentration and higher Seebeck coefficient (of $-200 \mu\text{V/K}$) were found [4]. This is probably due to the creation of Se vacancies during heating. Doping experiments on such materials have shown [15] that ZT can be improved, mainly by raising the power factor ($S^2\sigma$). More specifically, in Sn doped $K_2Bi_8Se_{13}$, the power factor was increased by a factor of ~ 3 compare to the pristine material [15].

In this work samples of $K_2Bi_8Se_{13}$ were prepared with three different synthetic conditions (see Table 1):

- Synthetic condition I: K_2Se and Bi_2Se_3 were initially mixed in 1/4 molar ratio. A slight excess of K_2Se (2–3%) was found necessary in order to obtain pure $K_2Bi_8Se_{13}$. This excess presumably compensated for the loss of K_2Se due to a reaction with silica tube that occurred during synthesis. For example, $K_2Bi_8Se_{13}$ was prepared by mixing 0.175 g K_2Se (1.1 mmol) and 2.830 g Bi_2Se_3 (4.3 mmol). Carbon coated silica tubes were used to inhibit glass attack by K_2Se . The reaction was performed in a silica tube sealed under vacuum in a tube furnace at $750\text{--}850^\circ\text{C}$ followed by cooling at a rate of $\sim 3^\circ\text{C/min}$.
- Synthetic condition II: K_2Se and Bi_2Se_3 were mixed as in synthetic condition I (Table 1) but the reaction was done by melting the constituents with a flame. This was followed by remelting the

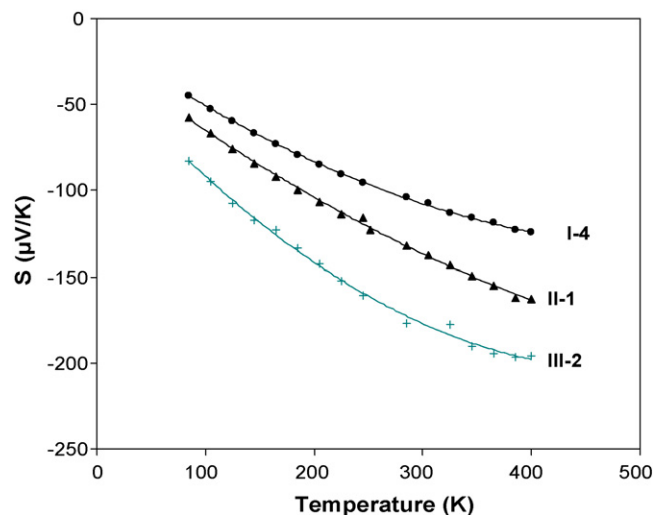


Fig. 4. Seebeck coefficient vs. temperature at 80–400 K for selected samples.

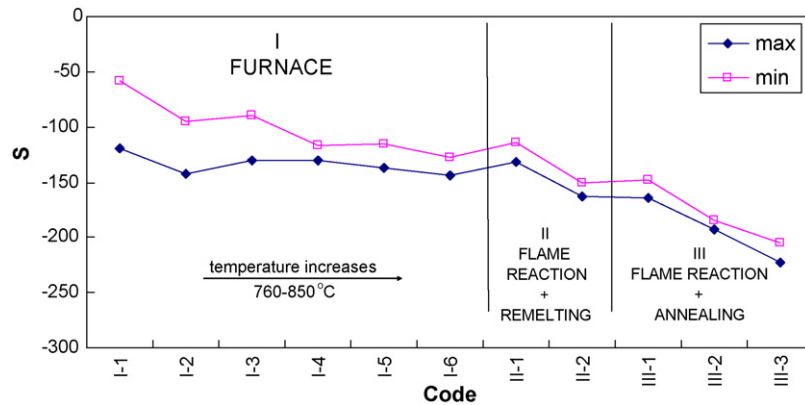


Fig. 5. Minimum and maximum room temperature Seebeck coefficient in a given batch for various conditions of synthesis.

material in a furnace. For the so-called “flame reaction” the tube was carefully placed under the flame of butane–propane mixture until the material melted. Then the tube was removed from the flame and quenched. The flame reaction has to be carried out by a cautious and experienced operator using protection shields and helmet. The products of the flame reaction were a mixture of $K_2Bi_8Se_{13}$ and $K_{2.5}Bi_{8.5}Se_{14}$ phases. To get pure $K_2Bi_8Se_{13}$ phase the sample was remelted in a furnace 750–850 °C followed by cooling with rate of ~ 3 °C/min.

- Synthetic condition III: K_2Se and Bi_2Se_3 were mixed as described above but the reaction was done by flame followed by annealing treatment under vacuum at 500 °C for more than 48 h. The products of the flame reaction were mixture of $K_2Bi_8Se_{13}$ and $K_{2.5}Bi_{8.5}Se_{14}$ phases and annealing at 400 °C was necessary to get pure $K_2Bi_8Se_{13}$ phase.

All products were pure $K_2Bi_8Se_{13}$ phase as judged by powder X-ray diffraction patterns that were compared to the calculated pattern using Cerius² software, see Fig. 2. Thermal differential scanning calorimetry (DSC) analysis showed a melting peak during heating at about 700 °C, see Fig. 3.

EDS analysis was used to obtain the elemental composition of the products. Table 2 shows the atomic percentage of the K, Bi and Se elements in the products of the three different categories. In order to improve limited accuracy by the EDS measurements, several points were measured and the average values are presented in Table 2. These results indicate an increasing trend of K percentage for synthetic condition III as well as an decreasing trend of Bi. This variation is expected to affect the doping level of the samples since K^+ and Bi^{3+} share the same crystallographic sites [4]. Excess K^+ ions are expected to act as acceptors, thus a lower carrier concentration in samples made with this synthetic condition is expected.

Table 2
EDS results for selected conditions of β - $K_2Bi_8Se_{13}$ synthesis

Sample	K (at.%)	Se (at.%)	Bi (at.%)
I-1	7.5	55.0	37.5
I-2	7.6	55.4	37.0
I-4	8.1	54.8	37.1
II-1	8.1	55.2	36.7
II-2	7.8	54.5	37.7
III-1	8.9	55.3	35.8
III-3	8.4	54.9	36.7

3.3. Properties of $K_2Bi_8Se_{13}$

Seebeck coefficient measurements and IR reflectivity spectra were carried out for samples prepared by all three types of synthetic conditions described above.

3.3.1. Seebeck coefficient

Seebeck coefficient was negative for all samples confirming the *n*-type character of the materials. It increases with temperature at the range of 80–400 K, see Fig. 4, and this behavior is typical of alkali bismuth selenide compounds [1].

In order to study the effect of synthetic conditions on doping homogeneity different samples obtained from the same ingot were measured. Fig. 5 shows the minimum and maximum values of Seebeck coefficient at room temperature that were taken from the same ingot. The variation of the Seebeck coefficient (difference between minimum and maximum value) was found to be decreased from I-1 to I-6. According to Table 1, the samples I-1 through I-6 were prepared at increasingly higher temperature, and the products are expected to be more homogeneous when prepared at higher temperatures. More homogeneous doping was also observed in samples obtained from the flame reaction (conditions II and III in Fig. 5).

Furthermore, there is a wide range of Seebeck coefficient values with various synthetic conditions (from sample I-1 through III-4 in

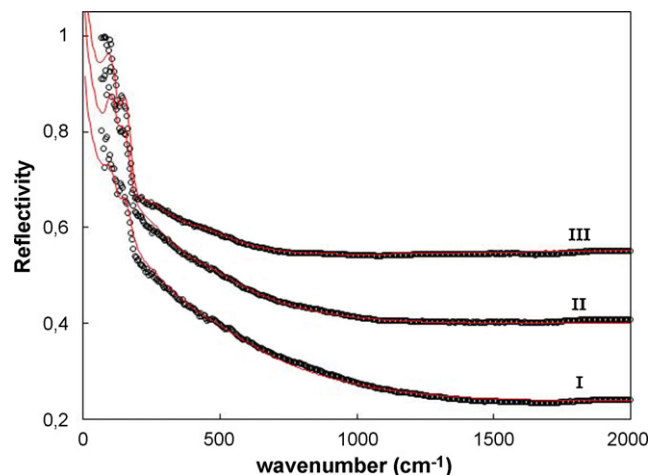


Fig. 6. Reflectivity data from pressed pellets of samples prepared with various synthetic conditions (I, II and III represent the sample categories shown in Table 1).

Fig. 5) suggesting a wide variation in the doping level. Regarding the Seebeck coefficient trends for different conditions these results show that

- the higher synthesis temperature, the higher the Seebeck coefficient
- the flame reaction produces samples with higher Seebeck coefficient especially when followed by annealing treatment.

3.3.2. Optical properties

IR reflectivity spectra in the far- and mid-infrared region on different $K_2Bi_8Se_{13}$ samples are shown in Fig. 6; the spectra are shifted along the y-axis for clarity. The spectra were analyzed by the Kramers–Kronig method and also fitted by classical dispersion theory [16,17]. The Kramers–Kronig (K–K) algorithm was optimised for increased accuracy in the high-end and low-end spectral regions. Fig. 7a shows a III-type sample where two zones are characteristic bands in the IR spectra at ~ 100 and ~ 150 – 160 cm^{-1} (see arrows in the inset). These are similar to those of other $K_2(Bi/Sb)_8Se_{13}$ compounds studied elsewhere [18]. There is a shoulder at about

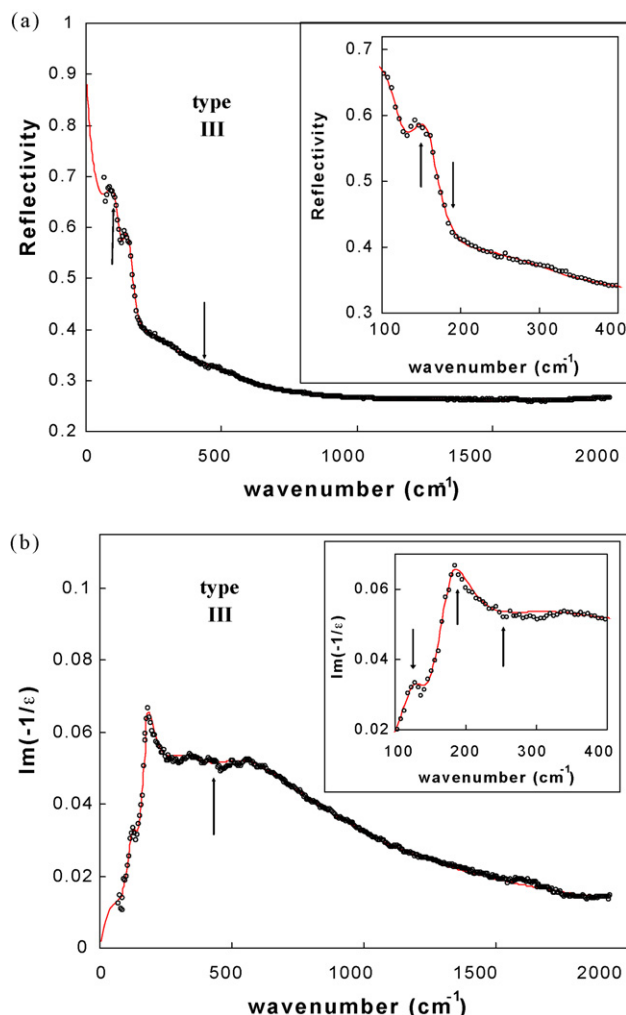


Fig. 7. Example of fitting results for the III-type of synthesis (a) reflectivity, (b) dielectric loss function $Im(-1/\epsilon)$. Point are the experimental data for reflectivity and K–K analysis for the $Im(-1/\epsilon)$. Solid lines represent the calculated curve from dispersion theory. In the inserts are shown the reflectivity and the dielectric loss function in short wavelengths. The arrows indicate the position of the TO-phonons (a) and LO-phonons (b).

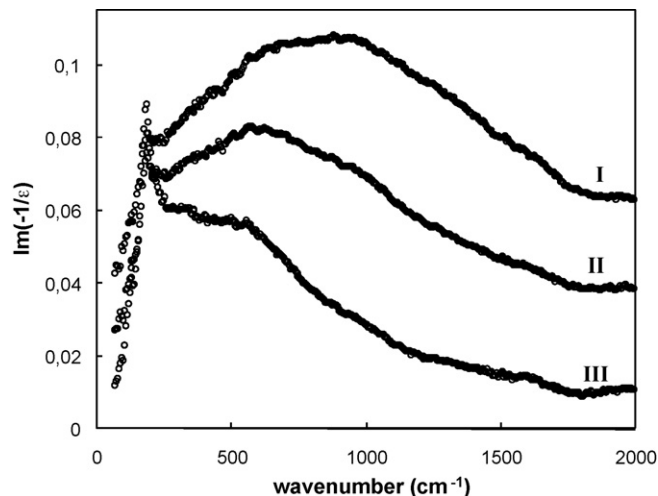


Fig. 8. Dielectric loss function, $Im(-1/\epsilon)$, for various synthesis conditions.

200 cm^{-1} (see arrows in the inset of Fig. 7a). The lines correspond to the analysis model that is described below.

Fig. 8 shows the dielectric loss function, $Im(-1/\epsilon)$, for the spectra, as obtained by K–K analysis. In the spectra of samples belonging to category III two clear peaks are observed (longitudinal optical (LO)-phonons) at about 130 and 180 cm^{-1} , see arrows in Fig. 7b, which are decreased at the expense of a broad band at higher wave numbers (at about 1070 cm^{-1} for spectrum of category I, Fig. 8).

The reflectivity $R(\omega)$ is given by [19]:

$$R(\omega) = \left| \frac{\sqrt{\epsilon(\omega)} - 1}{\sqrt{\epsilon(\omega)} + 1} \right|^2 \quad (1)$$

where $\epsilon(\omega)$ is the dielectric function. For the spectra analysis, we assume that dielectric function is given by [16]:

$$\epsilon(\omega) = \epsilon_{\infty} \left[\prod_j \frac{\omega_{LO,j}^2 - \omega^2 - i \cdot \gamma_{LO,j} \omega}{\omega_{TO,j}^2 - \omega^2 - i \cdot \gamma_{TO,j} \omega} - \frac{\omega_{PL}^2 - i \cdot (\gamma_P - \gamma_0) \omega}{\omega^2 + i \cdot \gamma_0 \omega} \right] \quad (2)$$

where ϵ_{∞} is the dielectric function at high frequencies and j is the number of modes. The first term in Eq. (2) that corresponds to the phonon contribution, proposed by Kurosawa [17], is the extension of the Lyddane–Sachs–Teller (LST) relation to finite frequencies, and works well in numerous cases, including strongly damped soft modes [20]. The second term corresponds to the free carrier contribution based on extended Drude model [21]. The frequencies $\omega_{LO,j}$ and $\omega_{TO,j}$ are the characteristic frequencies for longitudinal and transverse modes. The $\gamma_{LO,j}$ and $\gamma_{TO,j}$ are the damping factors for each mode j . Based on the Drude model γ_0 and γ_P are the damping constants for frequency $\omega = 0$ and $\omega = \omega_{PL}$ (plasma frequency), respectively. For $\gamma_0 = \gamma_P$ we obtain the known Drude equation. The plasma frequency (ω_{PL}) is given by

$$\omega_{PL}^2 = \frac{n \cdot e^2}{m^* \epsilon_0 \epsilon_{\infty}} \quad (3)$$

where ϵ_0 is the dielectric function of vacuum, m^* the carrier effective mass and n is the free carrier concentration.

The results of the analysis are shown in Fig. 9. For the analysis we assumed four modes with TO at 98.7, 148.4, 192.6 and 451.2 cm^{-1} and LO at 122.7, 171.6, 245.6 and 457.0 cm^{-1} . As an example, the results of the fit for a sample synthesized with condition III are shown in Fig. 7. As can be seen the overall fit is good for both the reflectivity spectrum and for the dielectric loss function $Im(-1/\epsilon)$. Similar fitting results were obtained for the spectra of all measured

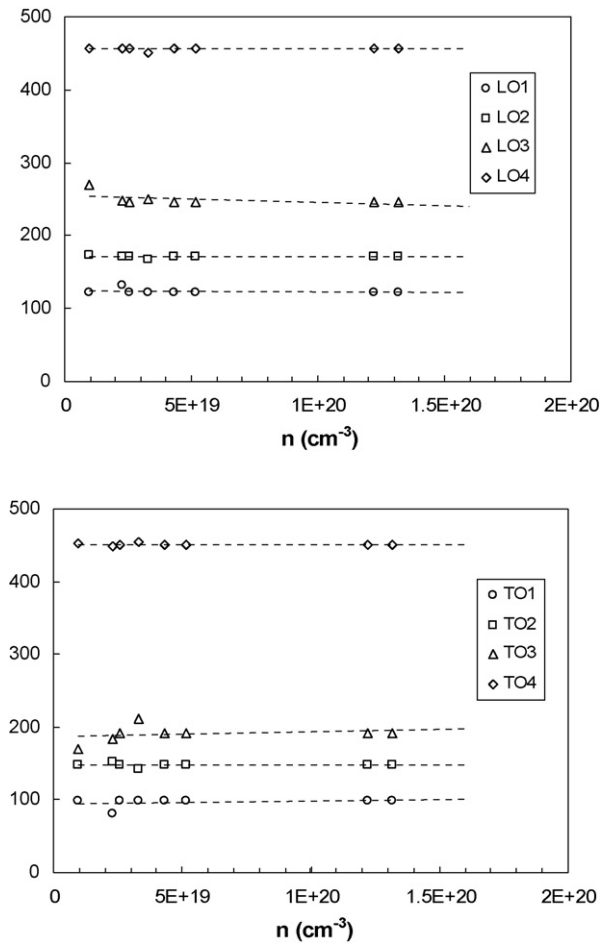


Fig. 9. TO and LO frequencies as a function of the free carrier concentration for different synthesis conditions.

samples. As shown in Fig. 9, the values of TO and LO frequencies remain practically unchanged, as expected. The change in the spectral characteristics of the dielectric loss function, $\text{Im}(-1/\epsilon)$, can be understood as due to the contribution of the free carrier concentration; actually, samples with higher free carrier concentration (as samples in synthesis type-I) show a more profound band at about 1070 cm^{-1} . This band is lowered in intensity and shifted into lower wavenumbers as the free carrier concentration is decreased.

From the analysis of the IR reflectivity spectra, it is evident that the plasmon is over-damped. The free carrier concentration was determined with Eq. (3), taking for simplicity the effective mass $m^* = 1$. As can be seen in Table 3, the various conditions of synthesis lead to samples with free carrier concentration ranging from 9.6×10^{18} to $1.3 \times 10^{20} \text{ cm}^{-3}$. The so-called “in furnace” reaction

Table 3

IR analysis results (plasma frequency, dumping factors and carrier concentration) for selected conditions of $\beta\text{-K}_2\text{Bi}_8\text{Se}_{13}$ synthesis

Sample	$\omega_p \text{ (cm}^{-1}\text{)}$	$\gamma_p \text{ (cm}^{-1}\text{)}$	$\gamma_0 \text{ (cm}^{-1}\text{)}$	$n \text{ (} 10^{19} \text{ cm}^{-3}\text{)}$
I-1	1068.9	2050.9	2050.9	12.2
I-2	1110.8	2490.8	2490.8	13.2
I-4	1102.8	2408.8	2408.8	13.2
II-1	632.4	1271.6	1039.8	4.29
II-2	700.4	1324.8	1180.6	5.18
III-1	464.9	955.6	955.6	2.30
III-2	300.2	609.9	609.9	0.96
III-3	461.0	1254.4	1254.4	2.56

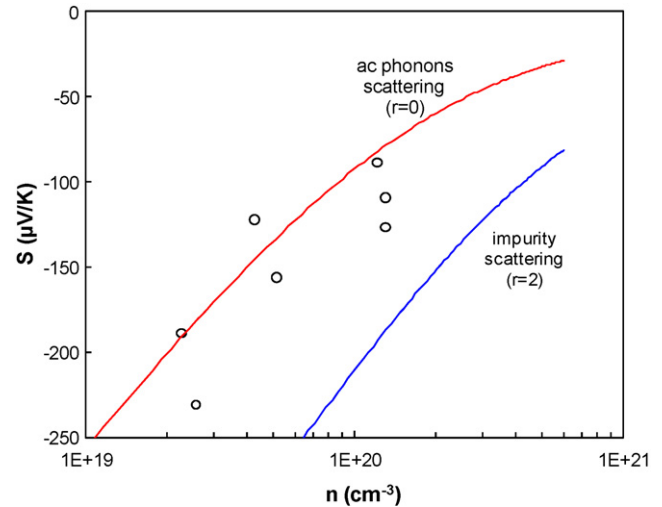


Fig. 10. Seebeck coefficient (average values from values in Fig. 5) vs. carrier concentration at room temperature. The solid lines are calculated based on Eq. (4) for assuming scattering by acoustic phonons ($r=0$) and by impurities ($r=2$).

(see Table 1) produces samples with high free carrier concentration of $1.2\text{--}1.3 \times 10^{20} \text{ cm}^{-3}$. The flame reaction followed by re-melting decreases the free carrier concentration ($5.1 \times 10^{19} \text{ cm}^{-3}$) by nearly a factor of two, while the free carrier concentration is again halved ($2.3\text{--}2.6 \times 10^{19} \text{ cm}^{-3}$) when annealing follows the flame reaction.

Fig. 10 shows the Seebeck coefficient with the carrier concentration. As expected from theory, when the free carrier concentration increases, the Seebeck coefficient should decrease. The Seebeck coefficient as well as the free carrier concentration depend on fermi level ($\eta = E_F/k_B T$ where E_F is the fermi level, k_B is the Boltzman constant and T is the temperature), through the fermi integrals. Seebeck coefficient and the free carrier concentration are given by [22]:

$$S = \pm \frac{k_B}{e} \left[\frac{F_{r+2}(\eta)}{F_{r+1}(\eta)} - \eta \right], \quad n = N_C \cdot F_{3/2}(\eta) \quad (4)$$

where e is the electron charge and N_C is the density of states in the conduction band. $F_r(\eta)$ are the fermi integrals, while the parameter r depends on the scattering mechanism ($r=0$ for acoustic phonon scattering, $r=2$ for impurities scattering), and are given by:

$$F_r(\eta) = \int_0^\infty \left(-\frac{\partial f(\epsilon, \eta)}{\partial \epsilon} \right) \cdot \epsilon^r d\epsilon \quad (5)$$

In the case of non-degeneracy, Eq. (4) is reduced to the well known formula [22]:

$$S = \pm \frac{k_B}{e} [A - \ln(n) + \ln(N_C)] \quad (6)$$

where A is related to scattering mechanisms ($A=2$ for acoustic phonon scattering, $A=4$ for ionized impurities scattering). As expected from theory, when the free carrier concentration increases, Seebeck coefficient should decrease. In a linear-log graph, in the case of a non-generate electron gas, the dependence of Seebeck coefficient to free carrier concentration should show a linear trend, with a slope k_B/e . In a more general case of arbitrary degeneracy, the dependence of the Seebeck coefficient on the carrier concentration should show a sub-linear trend (curved to higher n), as observed in Fig. 10. The solid lines in Fig. 10 are the calculated dependence based on Eq. (4) for reduced fermi level taken from -1 to 10 . Two extreme cases were considered, carriers are scattered by acoustic phonons ($r=0$) and by impurities ($r=2$). As shown in Fig. 10, the points lie well inside those two cases, indicative of a mixed scattering mechanism. From Fig. 10 we conclude that

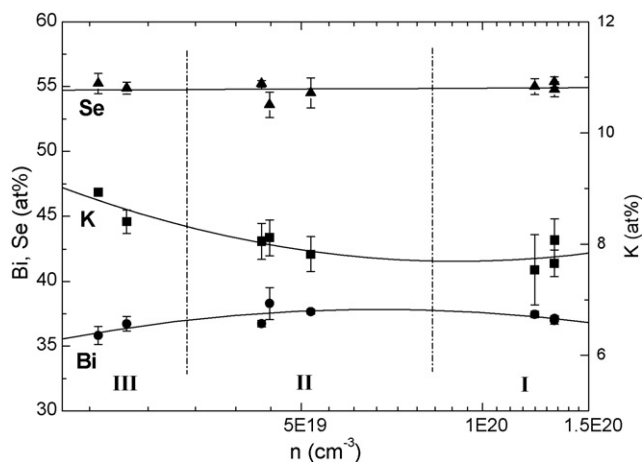


Fig. 11. EDS results for K, Bi and Se elemental analysis vs. log of carrier concentration. The error bars are based on the measurements of several points for each synthetic condition.

the electron gas in our samples should be degenerated to strongly degenerated.

Fig. 11 depicts how the free carrier concentration and sample stoichiometry are correlated. The ratio K^+/Bi^{3+} tend to increase as the carrier concentration decreases since more K and/or less Bi act as acceptors. Although the latter leads to a logical explanation based on conventional thinking on semiconductor doping (i.e., point defects in Bi_2Se_3 -type compounds [23]) in the present case the doping level is also strongly affected by the K/Bi disorder (mixed occupancy) as shown previously by band structure calculations [13]. We believe that the doping in these materials arises from more complicated factors including K/Bi substitution which varies from one synthetic condition to the next.

4. Conclusions

The results reported here show the strong relationship between the synthetic conditions of $K_2Bi_8Se_{13}$ and its doping level. Given the synthetic conditions, materials (see Table 1) with carrier concentration ranging from 9.6×10^{18} to $1.6 \times 10^{20} \text{ cm}^{-3}$ can be obtained. By comparison, the samples of $K_2Bi_8Se_{13}$ grown with the Bridgman technique [6] generally have high carrier concentration of $\sim 10^{20} \text{ cm}^{-3}$. The high carrier concentration was attributed to shallow donors that were formed in the material during Bridgman growth and seemed to be associated with the local disordering [11] between K and Bi. The wide carrier concentration range observed with different synthetic conditions is probably also due to changes and variation on the degree of local ordering between K and Bi as well as the variation on K^+/Bi^{3+} substitution although the ability to create Se vacancies, as is common in chalcogenides compounds [24,25], cannot be excluded. These results suggest that the carrier concentration in this system can be controlled to a certain degree. The flame reaction followed by annealing treatment seemed to be useful in giving lower carrier concentration and higher Seebeck coefficient which exceeds $-200 \mu\text{V/K}$.

More homogeneously doped samples with higher Seebeck coefficient were prepared by (a) the furnace method on higher synthesis temperatures and (b) the flame reaction method fol-

lowed by annealing. The work described here shows the response of $K_2Bi_8Se_{13}$ to synthetic conditions and the new information reported here can be exploited in future optimization procedures.

Acknowledgments

The authors thank Dr. E. Pavlidou for her help with EDS measurements. Cyprus Research Promotion Foundation is greatly acknowledged for the financial support (THEMATA–TEXNO/0104/16). MGK thanks ONR for support.

References

- [1] (a) M.G. Kanatzidis, *Semicond. Semimet.* 69 (2000) 51; (b) D.-Y. Chung, L. Iordanidis, K.-S. Choi, M.G. Kanatzidis, *Bull. Kor. Chem. Soc.* 19 (1998) 1283–1293; (c) M.G. Kanatzidis, *Chemistry, Physics and Materials Science of Thermoelectric Materials: Beyond Bismuth Telluride Fundamental Materials Science Series*, Kluwer Academic/Plenum Publishers, NY, 2003, pp. 35.
- [2] T.J. McCarthy, S.-P. Ngeyi, J.-H. Liao, D.C. DeGroot, J. Schindler, C.R. Kannewurf, M.G. Kanatzidis, *Chem. Mater.* 5 (1993) 331.
- [3] (a) Th. Kyratsi, J.S. Dyck, W. Chen, D.-Y. Chung, C. Uher, K.M. Paraskevopoulos, M.G. Kanatzidis, *Mater. Res. Soc. Symp. Proc.* 691 (2002) 419; (b) J.R. Ireland, Th. Kyratsi, M.G. Kanatzidis, C.R. Kannewurf, *Mater. Res. Soc. Symp. Proc.* 691 (2002) 431; (c) Th. Kyratsi, D.Y. Chung, J.S. Dyck, C. Uher, S. Lal, S. Loo, T. Hogan, J. Ireland, C.R. Kannewurf, E. Hatzikraniotis, K.M. Paraskevopoulos, M.G. Kanatzidis, *Mater. Res. Soc. Symp. Proc.* 793 (2003) 359; (d) Th. Kyratsi, D.-Y. Chung, J.S. Dyck, C. Uher, E. Hatzikraniotis, K.M. Paraskevopoulos, M.G. Kanatzidis, *Proceedings of 2nd European Conference on Thermoelectrics of the European Thermoelectric Society*, Kraków, Poland, 2004.
- [4] D.-Y. Chung, K.-S. Choi, L. Iordanidis, J.L. Schindler, P.M. Brazis, C.R. Kannewurf, B. Chen, S. Hu, C. Uher, M.G. Kanatzidis, *Chem. Mater.* 9 (12) (1997) 3060.
- [5] (a) G.A. Slack, *New Materials and Performance Limits for Thermoelectric Cooling*, in: D. Rowe (Ed.), *CRC Handbook of Thermoelectrics*, CRC Press, Inc, Boca Raton, FL, 1995, p. 407; (b) G.A. Slack, *The thermal conductivity of non-metallic materials*, in: H. Ehrenreich, F. Seitz, D. Turnbull (Eds.), *Solid State Physics*, vol. 34, Academic Press, New York, 1997, p. 1.
- [6] Th. Kyratsi, J.S. Dyck, W. Chen, D.-Y. Chung, C. Uher, K.M. Paraskevopoulos, M.G. Kanatzidis, *J. Appl. Phys.* 92 (2) (2002) 965.
- [7] Th. Kyratsi, D.-Y. Chung, M.G. Kanatzidis, *J. Alloys Compd.* 338 (2002) 36.
- [8] Th. Kyratsi, D.-Y. Chung, J.R. Ireland, C.R. Kannewurf, M.G. Kanatzidis, *Chem. Mater.* 15 (2003) 3035.
- [9] Th. Kyratsi, M.G. Kanatzidis, *Z. Anorg. Allg. Chem.* 629 (12) (2003) 2222.
- [10] D. Bilec, S.D. Mahanti, Th. Kyratsi, D.-Y. Chung, P. Larson, M.G. Kanatzidis, *Phys. Rev. B* 71 (8) (2005) 085116.
- [11] Th. Kyratsi, E. Hatzikraniotis, Ch. Malliakas, K.M. Paraskevopoulos, J.S. Dyck, C. Uher, M.G. Kanatzidis, *J. Appl. Phys.* 100 (2006) 123704.
- [12] CERIUSS², Version 2.35; Molecular Simulations Inc., Cambridge, UK 1995.
- [13] Th. Kyratsi, D.-Y. Chung, K.-S. Choi, J.S. Dyck, W. Chen, C. Uher, M.G. Kanatzidis, *Mater. Res. Soc. Symp. Proc.* 626 (2000) Z881.
- [14] Th. Kyratsi, S. Lal, T. Hogan, M.G. Kanatzidis, *Mater. Res. Soc. Proc. Symp.* 886 (2005) 275.
- [15] P.W. Brazis, M. Rocci-Lane, J.R. Ireland, D.-Y. Chung, M.G. Kanatzidis, C.R. Kannewurf, *Proceedings of the 18th International Conference on Thermoelectrics*, 1999, p. 619.
- [16] L. Genzel, A. Wittlin, M. Bauer, M. Cardona, E. Schonherr, A. Simon, *Phys. Rev. B* 40 (1989) 2170.
- [17] T. Kurosawa, *J. Phys. Soc. Jpn.* 16 (1963) 1298.
- [18] (a) E. Hatzikraniotis, Th. Kyratsi, T. Zorba, K.M. Paraskevopoulos, M.G. Kanatzidis, *Mater. Res. Soc. Symp. Proc.* 886 (2005) 269; (b) E. Hatzikraniotis, Th. Hassapis, Th. Kyratsi, K.M. Paraskevopoulos, M.G. Kanatzidis, *Proceedings of 25th International Conference on Thermoelectrics*, IEEE, Vienna, 2006, p. 573.
- [19] F. Gervais, B. Piriou, *Phys. Rev. B* 10 (1974) 1642.
- [20] D.W. Berreman, F.C. Unterwald, *Phys. Rev.* 174 (1968) 791.
- [21] J. Bouvier, N. Bontemps, M. Gabay, M. Nanot, F. Queyroux, *Phys. Rev. B* 45 (1992) 8065.
- [22] V.I. Fistul, *Heavily Doped Semiconductors*, Plenum Press, NY, 1969.
- [23] A. Vasko, L. Tichy, J. Horak, J. Weissenstein, *Appl. Phys. E* 5 (1974) 217.
- [24] P. Lostak, L. Benes, S. Civis, H. Sussmann, *J. Mater. Sci.* 25 (1990) 277.
- [25] I.F. Bogatyrev, A. Vasko, L. Tichy, J. Horak, *Phys. Stat. Sol. A* 22 (1974) K63.